

Validation of Fluid Flow and Solidification Simulation of a Continuous Thin-Slab Caster

Brian G. Thomas¹, Ron O'Malley², Tiebiao Shi¹, Ya Meng¹, David Creech¹,
and David Stone¹

¹ University of Illinois at Urbana-Champaign,
Department of Mechanical and Industrial Engineering,
1206 West Green Street, Urbana, IL USA, 61801
Ph: 217-333-6919; Fax: 217-244-6534; Email: bgthomas@uiuc.edu

² AK Steel Research
703 Curtis Street
Middletown, Ohio 45043
Ph: 513-727-5708; Fax: 513-727-5872; Email: Ronald.O'Malley@aksteel.com

Abstract

Models of fluid flow and solidification in the mold region of a continuous thin-slab caster have been developed and validated with extensive experimental measurements on the AK Steel - Mansfield stainless-steel caster. Three-dimensional turbulent flow of molten steel through the nozzle into the mold cavity is modeled with the finite difference code CFX 4.2, using the standard $K-\epsilon$ turbulence model and a fixed, structured grid. The results agree with flow measurements in a full-scale water model of the process. Next, the corresponding steady heat conduction equation is solved to predict the distribution of superheat in the molten pool. The predicted temperatures in the molten steel compare well with measurements conducted by inserting a thermocouple probe downward through the top surface at several locations in the operating thin slab caster. Next, solidification of the steel shell is simulated using a transient heat conduction model that features a detailed treatment of the flux layers in the interfacial gap and incorporates the superheat flux calculated from the fluid flow model. This model was calibrated with temperature measurements obtained from thermocouples in the copper mold during operation. It was run under the transient conditions present during a breakout. The predicted shell thickness profiles are compared with many shell thickness profiles measured around the perimeter of a breakout shell. Of greatest interest is the uneven thinning of the shell near the narrow face where the steel jet impinges, which is different between steady-state and the transient conditions of the breakout. This work demonstrates the quantitative ability of this modeling approach to simulate coupled fluid flow and solidification heat conduction in a real steel continuous casting process.

Introduction

As the modeling of casting processes matures, there is a growing need for documented evidence of the accuracy of the calculations. A good mechanistic model should demonstrate the ability to reproduce each of the different coupled phenomena involved and not just the end result. This can be done in part through analytical solutions to test problems, but the ultimate comparison with the real process is difficult. Simultaneous validation of fluid flow and solidification simulations is rarely attempted so is the subject of this work.

In this work, three-dimensional finite-difference models are applied to simulate turbulent fluid flow, heat transfer, and solidification in a continuous casting process for thin slabs of stainless steel. The conditions are chosen to match those at the AK Steel - Mansfield caster, where extensive measurements were available, including:

- velocities within the liquid pool (from water models)
- temperatures measured in the molten steel pool (plant trial)
- temperatures measured in the copper mold walls (mold thermocouples)
- heat flow rate (heat balance on the mold cooling water)
- thickness of the solidified steel shell (from breakout shell measurements)

The casting conditions include 132mm mold thickness, 965-984 mm mold width, 127 mm nozzle submergence depth (meniscus to top of port), 25.4 mm/s casting speed, and 57-61°C superheat for 434 stainless steel with 1502°C liquidus temperature. Further details on the plant measurements and conditions were reported at the previous MCWASP conference [1].

Computational Models

The fluid flow model solves the three-dimensional, single-phase steady Navier-Stokes equations and corresponding Eulerian heat conduction equation in the liquid pool using the standard K- ϵ turbulence model [2]. The computational domain, shown in Fig. 1, features a nozzle which delivers steel into the mold cavity through two side ports (angled 15° downward) and a bottom port (directed straight down). Symmetry was exploited by modeling only one quarter of the nozzle and mold. A structured grid of blocks with boundary-fitted coordinates was employed to mesh the entire complex geometry, shown in Fig. 1. Its construction required great care, but greatly decreased execution time relative to an unstructured grid. A grid of 294,317 nodes was found to adequately resolve both the velocity and temperature fields. Standard high-Re turbulent wall laws were employed at the boundaries, which correspond to the solidification front (fixed at the liquidus temperature). Temperature at the inlet was fixed to the pour temperature. The non-dimensional cell size at the wall, $y^+ = \rho C_\mu^{0.25} K^5 \mu^{-1} \Delta y$, was kept at about 30. Outlet pressure at the bottom of the domain was fixed to a constant while the normal gradients of all other variables were set to zero. The heat transfer wall law was implemented with a user subroutine [3]. The equations were solved using the finite-difference program CFX 4.2 [2] with under-relaxation factors between 0.3 and 0.7 (1.0 is successive substitution). To avoid sudden divergence, the cross-diffusion terms in the K and ϵ equations were deferred until the final 100 iterations, when their relaxation factors were increased linearly from 0 to 1 at the last iteration. The flow solution converged (momentum residuals $< 1 \times 10^{-4}$) in about 4000 iterations, which was followed by 500 additional iterations for the heat transfer solution. The complete computation required about 14 hours on a single Origin 2000 processor at NCSA. The velocity results were similar to those from a low Re K- ϵ simulation, although the temperature results were different. The low Re number model produced unreasonable results unless the grid was refined until $y^+ < 1$, which increased the grid size to more than 840,000 nodes. Further details on this model and the results are provided elsewhere [2, 3].

Solidification of the steel shell against the mold walls occurs just outside the flow model domain and is calculated using a one-dimensional transient finite-difference model of the mold, interface, and shell [4]. The nodal equations are solved on a fixed grid that moves downwards at the casting speed and can ignore axial conduction due to the high Peclet number. The vertical superheat flux profile calculated by the CFX model at a chosen location along the meniscus perimeter is imposed as a transient boundary condition on the solidifying shell model. Heat is extracted to the cooling water from the copper mold wall, which is modeled in the vertical direction using a 2-D steady-state analytical solution and in the width direction as a simple fin heat transfer surface. Heat transfer in the system is dominated by the thermal resistance of the interfacial gap. The model features detailed treatment of this gap, including a mass and momentum balance on the flux layers, knowing the consumption rate of the powder added to the top surface. Flux layer properties, interface resistances and solid flux velocities are obtained through calibration, while remaining consistent with measurements. Details of this model, CON1D, are given elsewhere [4].

Water Model Flow Pattern

The fluid flow conditions in the Mansfield mold were documented using a full-scale mold water model located at AK Steel's Research Center in Middletown, OH. The water model consists of a 1-meter deep tundish section with a motorized stopper rod assembly controlling flow through a production refractory SEN and well nozzle into a 2.6-meter long mold section with a Plexiglas® front. A false back and adjustable sidewalls are employed to allow thickness and width to be set to the casting conditions of interest (see Introduction). The water from the mold exit is recirculated back to the tundish inlet using a pump. Closed-loop control maintains constant water levels in the tundish and mold.

Fluid flow in the mold is visualized by injecting a small quantity of visible dye into the stopper rod well after steady-state conditions are achieved. Movement of the ink pulse was videotaped to record it exiting the SEN and circulating within the mold cavity. Average flow velocities were estimated by tracking the position of the dye interface on each successive video frame, fitting a second order polynomial to the position vs. time plot, and taking the derivative of the polynomial.

An example of the velocities measured in the water model is compared in Fig. 2 with the corresponding model simulations. Velocity along the center of the jet is predicted to be much larger than the average across the mold thickness, which is measured as the jet swirls and wanders within the mold cross section as it moves towards the narrow face. A photograph of the mold water model with the injected dye is shown in Figure 3. Superimposed on this figure is a plot of the velocity vectors in the centerline section. The flow pattern is a classic "double-roll" pattern as the jet traverses to the narrow face where it splits to flow upward (to the top surface and back towards the nozzle) and downward (to carry material deep into the caster). The jet angle (34° downward), impingement point, (340 mm below meniscus) and overall flow pattern predictions are reasonably accurate. Flow from the bottom port bends slightly towards the left, but this asymmetry is not simulated. The water model bottom also bends the lower recirculation region, but this is below the region of interest of this work.

Molten Steel Temperature

Temperature in the molten steel pool is difficult to measure and rarely reported. Vertical temperature profiles in the Mansfield caster were measured for this work by constructing an apparatus to lower a thermocouple probe down through the top surface powder and slag layers into the flowing molten steel. The probe is lowered slowly (0.6 mm per s) to allow time for thermal equilibrium. After reaching its maximum depth of 180 mm, the probe is raised back up and withdrawn from the top. A slight hysteresis occurs between immersion and withdrawal, which obscures the exact position of the liquid slag / steel boundary.

An example of the measurements obtained with the probe are presented in Fig. 4. Results are presented in terms of the superheat temperature, which is the difference between the pour temperature measured in the tundish just above the outlet and the liquidus temperature. For this flow pattern, the temperature is relatively constant with depth at about 29% of the superheat. The model calculations almost match the measurements within the natural measured variation. A slight dip in the temperatures is predicted when the depth reaches the center of the upper recirculation region. This is shown more clearly in the temperature contour plot in Fig. 5, which is calculated by the 3-D CFX model. This slight dip could not be distinguished in the measurements, likely due to the turbulent fluctuations.

As the steel flows in the liquid pool, it transfers its superheat across the boundaries of the flow domain into the solidifying steel shell. The superheat flux delivered to the shell reaches a peak where the jet impinges on the narrow face shell wall, as shown in Fig. 6. A lesser peak occurs lower down on the wide face wall, where the bottom jet impinges. The accuracy of this prediction is suggested in part by the agreement of the liquid temperatures. Of greater significance is the effect of this superheat flux on the solidifying steel shell, predicted later.

Mold Wall Temperature and Cooling Water Heat Balance

The solidification model, CON1D, was calibrated by adjusting interface heat transfer parameters until the calculated total heat removed in the mold matched that based on the measured temperature rise of the cooling water. Further adjustments were made to ensure that the relative heat removal rates along the mold length allowed the temperatures calculated in the mold wall to match the measurements as well. Slight differences in the solid flux velocity profile were employed between the narrow face and wide face simulations, in order to match the separate measurements obtained for each mold face.

Because the mold geometry near the thermocouple is complicated, a three-dimensional finite element model of a portion of the mold wall was developed to determine the difference between the actual temperature expected at the thermocouple location and the value predicted by the simple one-dimensional CON1D, for a given heat flux. A typical set of test conditions and 3-D results is shown in Fig. 7. The temperatures from CON1D were found to match those in the 3-D models if the thermocouple position was adjusted by offsetting it towards the hot face by 11.4 mm (narrow-face) or 3-5 mm (wide-face). This offset was then used for subsequent calculations.

A comparison between measured temperatures in the mold wall and predictions (using the offset) is shown in Fig. 8 for the central region of the wide face. This agreement is expected and indicates the extent of model calibration and the consistency between the mold thermocouple and cooling water temperature measurements.

Breakout Shell Thickness

Having established both the heat extracted to the mold wall and the heat supplied to the solidification front from the liquid superheat, no significant uncertainties remain for the heat transfer analysis of the solidifying steel shell under steady-state conditions. To validate the predictions, comparisons were made with thickness measurements on a breakout shell. The breakout occurred at the Mansfield caster under similar casting conditions to those for the previous measurements presented. Analysis of a breakout is complicated because it always occurs under transient conditions, when the casting speed and mold level both drop with time. The history of this particular breakout was documented carefully [1] so that it could be simulated using transient calculations with CON1D.

The predicted and measured shell thickness profiles are presented in Figs. 10 and 11, where it can be seen that reasonable agreement is obtained, assuming a solid fraction of 0.1 to define the shell. Thinning along the narrow face is observed. The region of maximum thinning is expected near the vicinity of jet impingement, but is observed slightly higher up the breakout shell when transient conditions are taken into account. It is interesting to note that the initial increase in thickness at the top of the breakout shell is much steeper than predicted under steady conditions. This is a natural consequence of the liquid level dropping while the shell is withdrawn, which allows the top of the breakout shell more solidification time than experienced under steady conditions.

Conclusions

An efficient model of 3-D turbulent flow and solidification in a thin slab caster has been developed. The model features one-way coupling between a K- ϵ flow model (CFX) and a 1-D transient model of heat transfer in the mold, interface, and solidifying steel shell (CON1D). The accuracy of this modeling approach has been demonstrated by comparison with experimental measurements of fluid flow in the liquid pool, temperature in the molten steel, temperature in the copper mold walls, temperature increase of the cooling water, and breakout shell thickness.

These modeling tools can now be applied to study related phenomena of practical significance in a quantitative manner. These include ideal taper of the mold walls to match the shell shrinkage, the critical shell thickness to avoid breakouts, the behavior of flux layers in the interfacial gap, the formation of cracks, and the development of relationships between mold wall temperatures and events in the solidifying shell to enable online quality prediction.

References

1. B.G. Thomas, R.J. O'Malley and D.T. Stone, (1998), "Measurement of temperature, solidification, and microstructure in a continuous cast thin slab", Proceedings of Modeling of Casting, Welding, and Advanced Solidification Processes VIII, The Minerals, Metals, and Materials Society, Warrendale, PA, 1185-1199.
2. AEA Technology, (1998), "CFX 4.2" Users Manual, (1700 N. Highland Rd., Suite 400, Pittsburgh, PA 15241).
3. D. Creech, (1998), "Computational Modeling of Multiphase Turbulent Fluid Flow and Heat Transfer in the Continuous Slab Casting Mold" (M.S. Thesis, Univ. of Illinois).
4. B.G. Thomas, B. Ho and G. Li, (1998), "Heat Flow Model of the Continuous Slab Casting Mold, Interface, and Shell," Alex McLean Symposium Proceedings, Iron & Steel Society, 177-193.

Acknowledgements

This work was supported by the Continuous Casting Consortium at UIUC, (AK Steel, Allegheny Ludlum, Columbus Stainless, Ispat-Inland Steel, LTV, and Stollberg, Inc.) and the National Science Foundation (Grant DMI-98-00274). The authors also wish to thank the National Center for Supercomputing Applications at UIUC for computing time and use of CFX; AK Steel for the water model and plant measurements, and M. Langeneckert and G. Webster for their roles in finite element analysis of the mold.

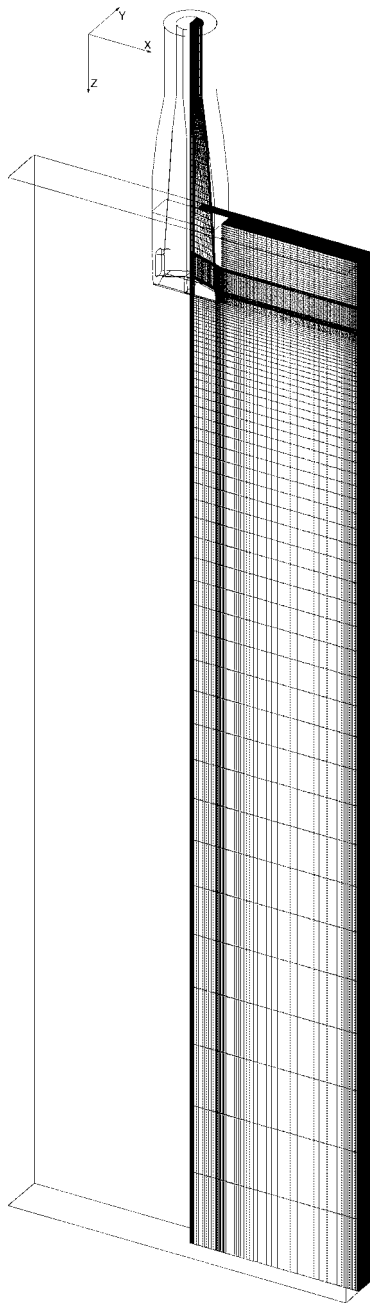


Figure 1: Domain and Mesh for 3D Flow and Heat Transfer Simulation of Continuous Casting Mold for Thin Slabs

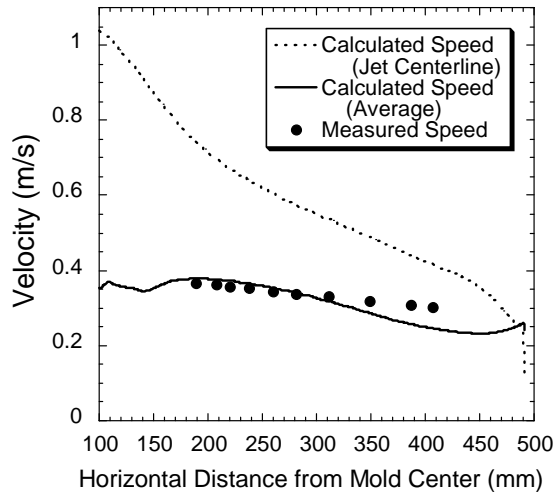


Figure 2: Velocity Along Flowing Jet (Calculated and Water Model Measurements)

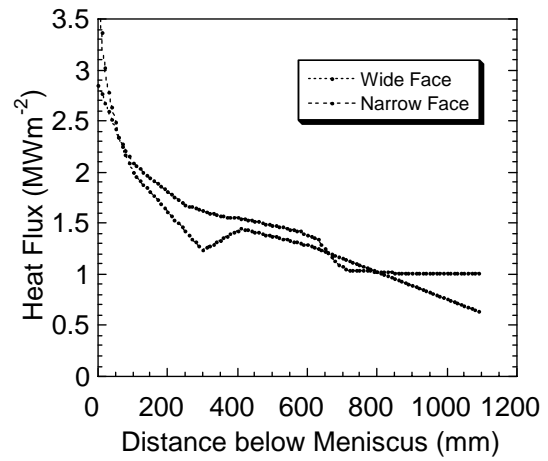


Figure 9: Heat Flux Profiles Calculated Between Strand and Mold Walls

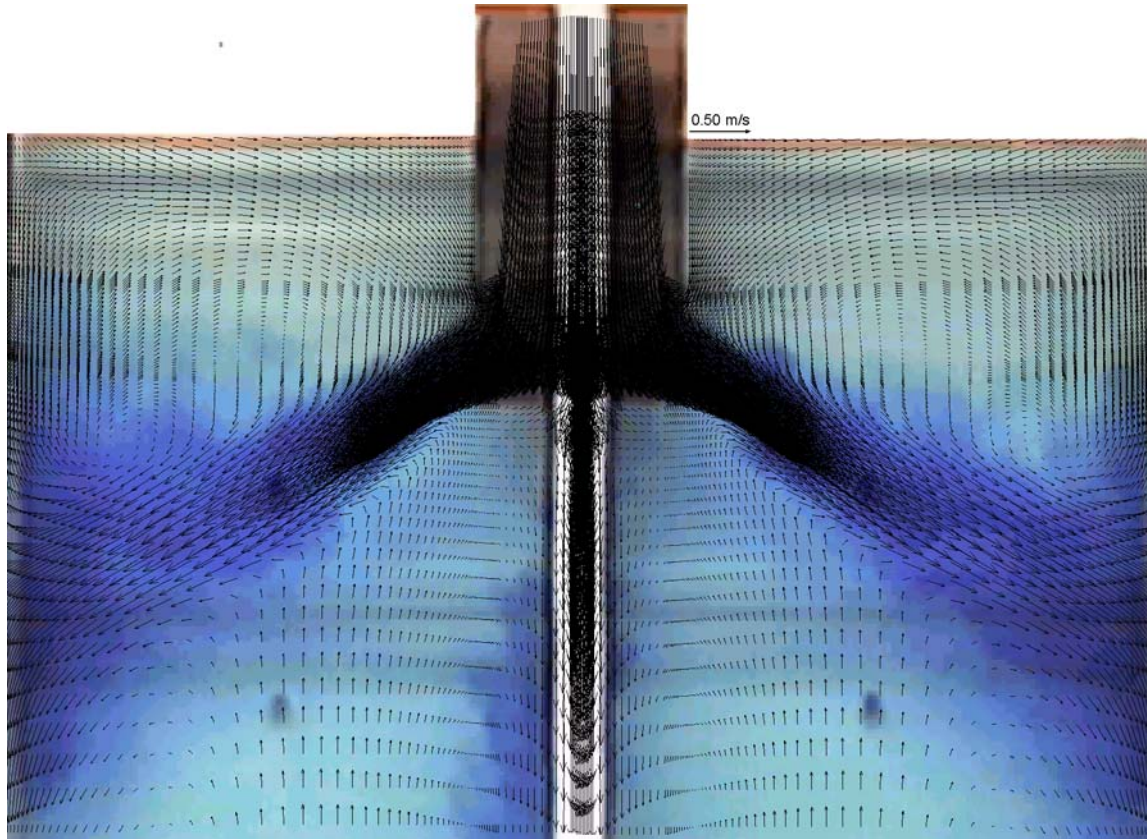


Figure 3: Calculated Velocity Vectors Superimposed on Water Model During Die Injection

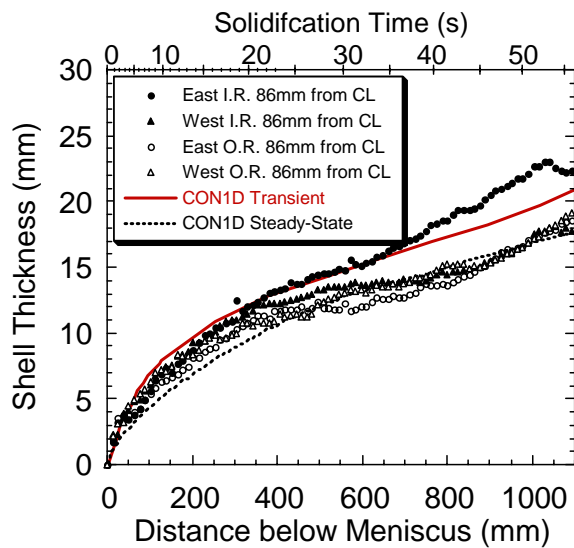


Figure 10: Shell Thickness Along Wide Face (Calculated Compared with Breakout Shell Measurements)

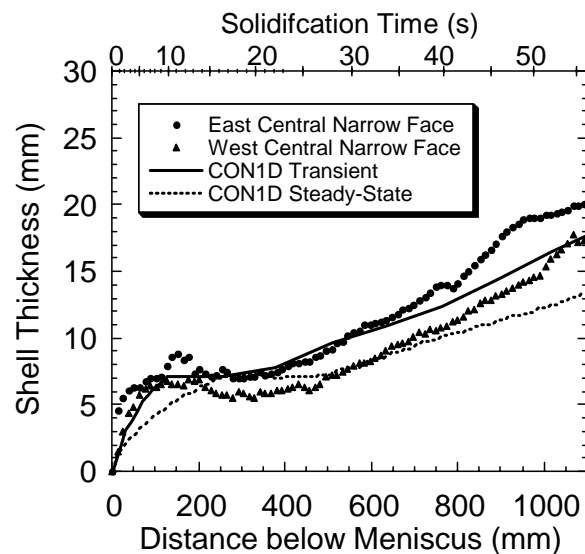


Figure 11: Shell Thickness Along Narrow Face (Calculated Compared with Breakout Shell Measurements)

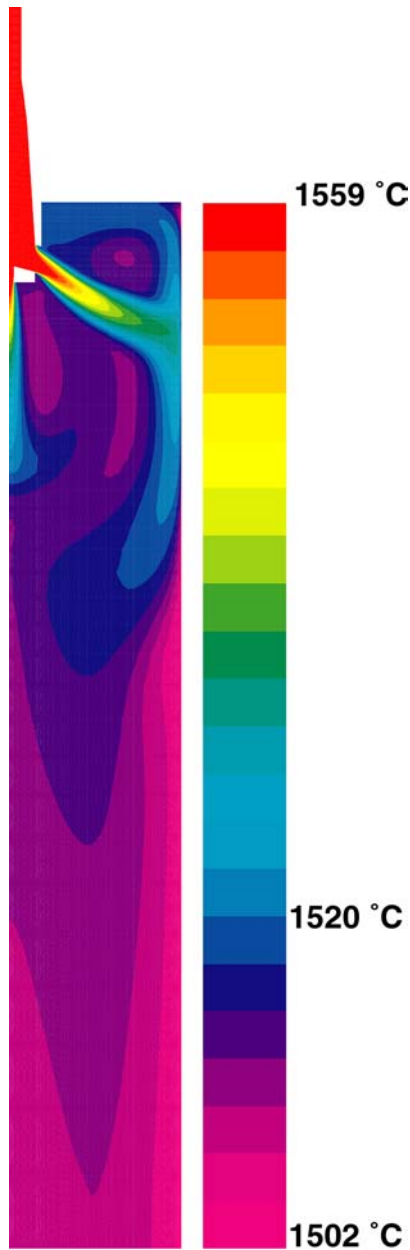


Figure 5: Temperature Contours Calculated in Molten Steel Pool

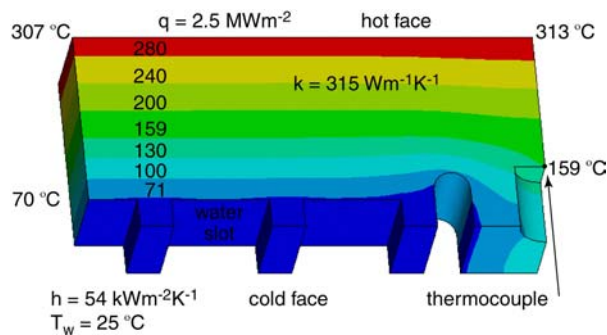


Figure 7: Temperature Contours in 3-D Portion of Mold Wall Showing Thermocouple Position & Temperature for Test Conditions

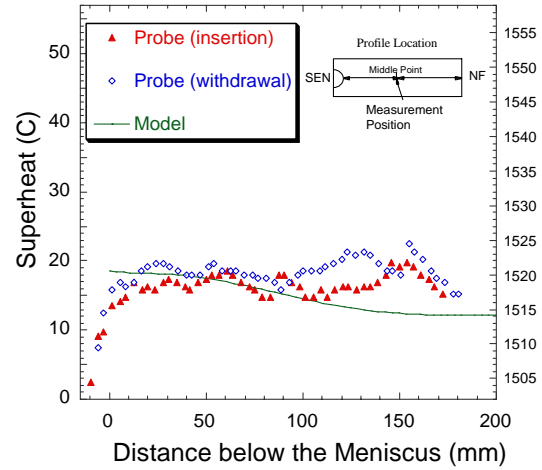


Figure 4: Temperature in Molten Steel (Measurements Compared with Calculations)

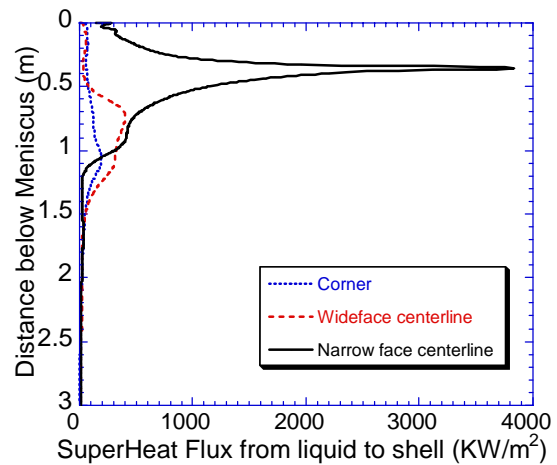


Figure 6: Superheat Flux Profiles Around the Exterior of the Strand Surface

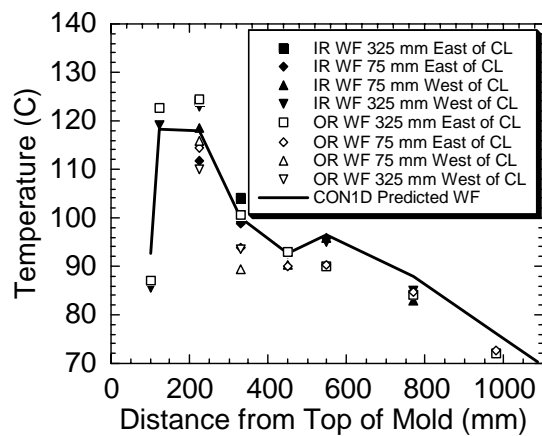


Figure 8: Temperatures Down Wide Face Mold Wall (Calculated and Measured)